PAPER • OPEN ACCESS

Simulating general relativity and non-commutative geometry by non-paraxial quantum fluids

To cite this article: Giulia Marcucci and Claudio Conti 2019 *New J. Phys.* **21** 123038

New Journal of Physics
The open access journal at the forefront of physics

Deutsche Physikalische Gesellschaft DPG
IOP Institute of Physics

Published in partnership with: Deutsche Physikalische Gesellschaft and the Institute of Physics

OPEN ACCESS

RECEIVED
19 August 2019

REVISED
21 November 2019

ACCEPTED FOR PUBLICATION
29 November 2019

PUBLISHED
17 December 2019

PAPER

Simulating general relativity and non-commutative geometry by non-paraxial quantum fluids

Giulia Marcucci[1,2] **and Claudio Conti**[1,2]

[1] Department of Physics, University Sapienza, Piazzale Aldo Moro 2, I-00185 Rome, Italy
[2] Institute for Complex Systems, National Research Council (ISC-CNR), Via dei Taurini 19, I-00185 Rome, Italy

E-mail: claudio.conti@uniroma1.it

Keywords: nonlinear optics, quantum simulation, analog gravity, spatial solitons

Abstract

We show that quantum fluids enable experimental analogs of relativistic orbital precession in the presence of non-paraxial effects. The analysis is performed by the hydrodynamic limit of the Schrödinger equation. The non-commutating variables in the phase-space produce a precession and an acceleration of the orbital motion. The precession of the orbit is formally identical to the famous orbital precession of the perihelion of Mercury used by Einstein to validate the corrections of general relativity to Newton's theory. In our case, the corrections are due to the modified uncertainty principle. The results may enable novel relativistic analogs in the laboratory, also including sub-Planckian phenomenology.

1. Introduction

Quantum simulations of fundamental theories realize novel tests and investigations of inaccessible physical regimes. The phenomenology of the fundamental laws of physics modified at the Planck scale attracts a large community of scientists [1–7]. The challenge is to identify feasible experiments to test the apparently inaccessible limits of quantum mechanics and general relativity [8]. The difficulties in realizing such large-scale experiments trigger studying quantum simulations. The simulations are realizable in Earth-based laboratories in a human-life timescale. Researchers aim at realizing analog experimental models of black holes [9–11], Hawking radiation [12–15], inflation and universe expansion [16, 17], dark-matter models [18], and related phenomena [19–21]. The analogy is a fundamental tool in physics, and experimental and theoretical analogs may deepen our understanding of quantum gravity theories [22], and of other challenging proposals as time-asymmetric quantum mechanics [23–25]. All the considered quantum simulations in optics are limited to the paraxial regimes. Despite this enables to simulate interesting physics, the use of non-paraxial effects is so far unexplored.

In this manuscript, we study the orbital precession of a quantum fluid (figure 1(a)) due to the perturbation to quantum mechanics analog models induced by non-paraxial terms Quantum fluids are studied in the vast literature concerning Bose–Einstein condensates (BECs), classical and quantum nonlinear optics and polaritonics [26–30]. We consider a quantum fluid wave-packet with a non-vanishing angular momentum in a trapping potential. We show that the wave-packet elliptical orbit is perturbed by the new terms, and we find a direct analog of the orbital precession induced by post-Newtonian gravitation. The dynamics is equivalent to the known treatment of the precession of Mercury in general relativity [31–33].

We also find a very interesting connection with the study related to the Generalized Uncertainty Principle (GUP), considered in sub-Planckian physics. Surprisingly enough, the orbital precession may also be explained in terms of non-commuting variables, as those that arise in studies in quantum gravity [34]. A large amount of literature deals with modifications of the uncertainty principle and related non-commutative geometry [35]. In standard quantum mechanics, there is no minimal value for the position uncertainty ΔX. However, theories in quantum gravity imply the existence of a minimal length scale, commonly identified with the Planck length $\ell_{\rm P}$ [1]. Hence a lower bound for ΔX must be included in quantum mechanics, and the Heisenberg relation $\Delta X \Delta P \geqslant \hbar/2$, with the momentum uncertainty ΔP, must be generalized—also in the non-relativistic limit

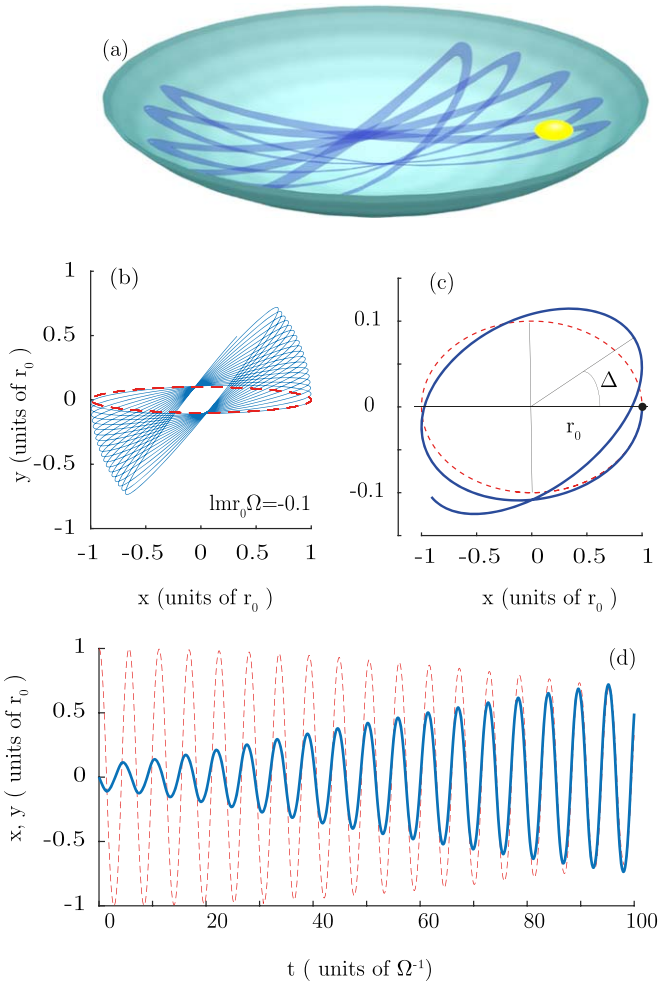

Figure 1. (a) A quantum-fluid wave-packet (yellow) in an elliptical orbit in a parabolic potential; the non-paraxial perturbations to the standard non-relativistic quantum mechanics induce a orbital precession; (b) solutions of equation (10) with $lmr_0\Omega = -0.1$, $\beta(m r_0\Omega)^2 = 0.1$ (continuous line) and $\beta = 0$ (dashed line) with Ωt in the range [0, 100]; (c) as in (a) for $\Omega t \leqslant 8$, the dot indicates the initial position; (d) x (dashed line) and y versus time t.

considered hereafter. The most accepted formulation of the so-called modified or GUP reads [36, 37]

$$\Delta X \Delta P > \frac{\hbar}{2}(1 + \beta \Delta P^2). \tag{1}$$

Equation (1) implies $\Delta X > \hbar\sqrt{\beta}$ with β a unknown constant, which is eventually related to ℓ_P. We need experimental evidence to assess the validity of equation (1) and fix bounds for the value of β. The GUP in equation (1) arises in a theory-independent way. Many theories attempting to unify gravity and quantum mechanics—including string theory [38]—predict modifications of the Heisenberg principle as in equation (1). The GUP is also related to modified commutation relations and to non-commutative theories [34, 39–42]. The GUP has many implications as, for example, in cosmological dynamics, black-body radiation, wave-packet localization and related investigations reported by several authors [42–46]. Quantitative bounds for the β parameter in the modified Heisenberg principle in equation (1) were also reported [45]. Other authors discussed human-scale laboratory tests with optomechanical and orbiting classical objects [47–50]. However, the application of generalized quantum mechanics to the macroscopic world is questionable [40].

Analogs, i.e. physical systems governed by laws mathematically identical to those of the generalized quantum mechanics, were considered in the fields of optics and relativistic BECs [51–55]. The fact that non-paraxial quantum fluids enable the simulations of non-commutative quantum mechanics, and general relativistic effects, opens several possibilities for studying analogs of unexplored phenomena in the laboratory.

2. Non-paraxial Schrödinger equation (SE)

We study the generalized SE for quantum fluids with trapping potential V in two or three spatial dimensions

$$\imath\hbar\frac{\partial\psi}{\partial t} = -\frac{\hbar^2}{2m}\nabla^2\psi + \frac{\beta\hbar^4}{m}\nabla^4\psi + V(\mathbf{r})\psi = \hat{H}\psi. \tag{2}$$

Equation (2) describes a non-interacting atomic BEC, realized by employing the Feshbach resonance [56]. Equation (2) also describes a polaritonic or photonic condensate. In the latter case, as extensively discussed in the literature, t corresponds to the propagation direction, and $\hbar$ must be replaced by the reduced light wavelength $\lambda/2\pi$ [57] equation (2) contains a kinetic term weighted by β. As considered by various authors [45, 52, 58], the additional kinetic term is the simplest modification to the SE that implies the GUP in equation (1) and arises from fundamental modifications to the geometry of the space-time at the Planck scale, which change the dispersion relation of free particles, as photons. In the optical case, corrections to paraxial approximation introduce the $\nabla^4\psi$ term, and the ratio between λ and the beam waist determines β in a optical analog to the generalized quantum mechanics [52]. For cold atoms, higher order derivatives may arise from relativistic effects (not considered here), when the fluid velocity is comparable with the velocity of light c [59]. Another mechanism is the modification of the dispersion relation in models as doubly-special-relativity [60].

Letting $\hat{p} = -\imath\hbar\nabla$, the Hamiltonian in equation (2) is

$$\hat{H} = \frac{\hat{p}^2}{2m} + \frac{\beta}{m}\hat{p}^4 + V(\mathbf{r}) \tag{3}$$

with the position vector $\mathbf{r} = (x, y, z) = (x^1, x^2, x^3)$. One introduces non-commutative coordinates by a new set of 'high-energy' variables (X^μ, P^μ), which, in the simplest case considered here, read $(\mu, \nu = 1, 2, 3)$

$$\begin{aligned}\hat{X}^\mu &= \hat{x}^\mu;\\ \hat{P}^\nu &= \hat{p}^\nu(1 + \beta\hat{p}^2).\end{aligned} \tag{4}$$

By $[\hat{x}^\mu, \hat{x}^\nu] = 0, [\hat{p}^\mu, \hat{p}^\nu] = 0, [\hat{x}^\mu, \hat{p}^\nu] = \imath\hbar\delta^{\mu,\nu}$, one has $[\hat{P}^\mu, \hat{P}^\nu] = [\hat{X}^\mu, \hat{X}^\nu] = 0$ and [45, 50, 61]

$$[\hat{X}^\mu, \hat{P}^\nu] = \imath\hbar\,(\delta^{\mu\nu} + \beta\delta^{\mu\nu}\hat{P}^2 + 2\beta\hat{P}^\mu\hat{P}^\nu). \tag{5}$$

This represents a weak version of non-commutative phase-space coordinates: at variance with standard quantum mechanics, the momentum and the position in different directions do not commute [34]. The standard case involves also commutation relations between position coordinates.

By $\hat{P}^\mu$, equation (2) has the traditional form

$$\imath\hbar\psi_t = \frac{\hat{P}^2}{2m}\psi + V(\mathbf{r})\psi, \tag{6}$$

but the commutation relations are modified and equation (1) holds true. The simplest effect of the additional kinetic term are shifts ΔE_k in the energetic levels of the eigenstates [62], $\Delta E_k = \frac{\beta}{m}\langle k|\hat{p}^4|k\rangle = 4m\beta\,\langle k|V^2|k\rangle$. Such perturbations may eventually occur in optical and atomic quantum fluids, however they are very difficult to observe [45]. We consider a more accessible phenomenology related to the dynamics of a wave-packet orbiting in the potential.

3. Hydrodynamic limit and Hamilton equations

We study a wave-packet initially located at $r = \sqrt{x^2 + y^2} = r_0$ that rotates with a non-vanishing angular momentum (figure 1(a)). The trajectory is found in the hydrodynamic approximation [63, 64] by letting $\psi = A\exp(\imath\mathcal{S}/\hbar)$ with $\hbar \to 0$ [65]. The Hamilton–Jacobi equation for $\mathcal{S}$ is [66, 67]

$$\frac{\partial\mathcal{S}}{\partial t} + \frac{(\nabla\mathcal{S})^2}{2m} + \frac{\beta}{m}(\nabla\mathcal{S})^4 + V = 0. \tag{7}$$

By the classical Hamiltonian $H(\mathbf{q}, \mathbf{p}) = \mathrm{p}^2/2m + (\beta/m)p^4 + V$, we have $\partial_t\mathcal{S} + H(\mathbf{q}, \nabla\mathcal{S}) = 0$. Equation (7) is solved by the Hamilton system with $\mathbf{p} = \nabla\mathcal{S}$ [67]

$$\begin{aligned}\frac{\mathrm{d}\mathbf{q}}{\mathrm{d}t} &= \nabla_p H,\\ \frac{\mathrm{d}\mathbf{p}}{\mathrm{d}t} &= -\nabla_q H.\end{aligned} \tag{8}$$

We consider here a *z-independent* radial potential with polar symmetry: $V = V(r)$. Two-dimensional condensates are routinely considered in the literature [27, 30, 65]. In polar coordinates (r, θ, z), with conjugate momenta (p_r, p_θ, p_z), we have

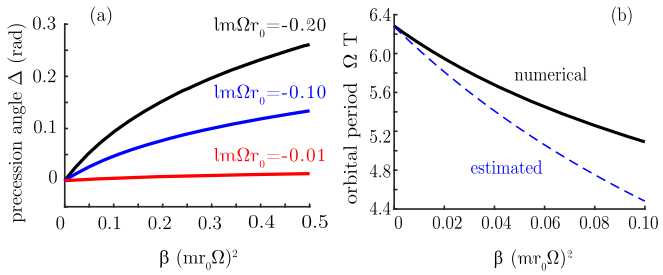

Figure 2. Effect of the perturbation β to the uncertainty principle in equation (1) on the (a) precession angle Δ for various l and (b) orbital period T for $lm\Omega r_0 = 1.01$, the dashed line is the theoretical estimate (see text).

$$H = \frac{1}{2m}\left(p_r^2 + \frac{p_\theta^2}{r^2}\right) + \frac{\beta}{m}\left(p_r^2 + \frac{p_\theta^2}{r^2}\right)^2 + V(r). \tag{9}$$

The corresponding Lagrangian does not depend explicitly on θ, hence the conjugate momentum $p_\theta = l$ is conserved, and the motion occurs in the z plane, with $p_z = 0$. By the conserved l, equation (8) are written as

$$\begin{aligned}
&\frac{\mathrm{d}\theta}{\mathrm{d}t} = \frac{l}{mr^2}\left[1 + 4\beta\left(p_r^2 + \frac{l^2}{r^2}\right)\right], \frac{\mathrm{d}p_\theta}{\mathrm{d}t} = 0,\\
&\frac{\mathrm{d}r}{\mathrm{d}t} = \frac{p_r}{m}\left[1 + 4\beta\left(p_r^2 + \frac{l^2}{r^2}\right)\right], \frac{\mathrm{d}p_r}{\mathrm{d}t} = -\frac{\partial H}{\partial r} = -V'(r) + \frac{l^2}{mr^3}\left[1 + 4\beta\left(p_r^2 + \frac{l^2}{r^2}\right)\right],
\end{aligned} \tag{10}$$

with $V' = \mathrm{d}V/\mathrm{d}r$ and, for a parabolic potential,

$$V = \frac{1}{2}m\Omega^2 r^2. \tag{11}$$

4. Orbital precession and link with the Einstein solution

Figure 1(b) shows the numerical solutions of equation (10) with $r(0) = r_0$ and $p_r(0) = 0$. When $\beta = 0$ and $l \neq 0$, the orbit is elliptical (dashed line in figure 1(b)). When $\beta > 0$—continuous line in figure 1(a)—the orbit exhibits a precession (clockwise for $l < 0$, and counter-clockwise for $l > 0$). Figure 1(c) shows the precession angle Δ with the particle at $t = 0, x = r_0$ and $y = 0$.

As the orbit rotates, the maximal position in the y coordinate is amplified as shown in figure 1(d). This orbital enhancement of the quantum gravity effect resembles the known gravity slingshot assist adopted to alter the speed of a spacecraft in orbital mechanics [68]: the radial acceleration at any turn emphasizes the phenomenology.

We remark that the precession can be related to non-commutative coordinates in the phase-space that arise because of the quantum gravity terms If we introduce the classical counter-part of the generalized momenta (4),

$$P_{r,\theta} = p_{r,\theta}(1 + \beta p^2) \tag{12}$$

the Hamiltonian H is written as in the case $\beta = 0$:

$$H = \frac{1}{2m}\left(P_r^2 + \frac{P_\theta^2}{r^2}\right) + V(r). \tag{13}$$

However, while the Poisson brackets $\{r, p_\theta\} = \{\theta, p_r\} = 0$ vanish [67], the corresponding quantities for the generalized momenta are

$$\{r, P_\theta\} = r^2\{\theta, P_r\} = 2\beta P_r P_\theta. \tag{14}$$

Therefore, one has modified mechanics with non-commuting coordinates. In the following, we show that the precession is of the order of magnitude of the brackets in equation (14), revealing the link between the non-commutative geometry and GUP phenomenology.

Equation (10) give the precession angle Δ by $\mathrm{d}\theta/\mathrm{d}r = l/[p_r(r)r^2]$ with $p_r(r)$ expressed in terms of the conserved quantities $H = E_0$ and $p_\theta = l$. However, no closed form can be found, and figure 2 shows numerical results. We obtain estimates by considering a nearly circular orbit with $r \simeq r_0$. If $\beta = 0$, then $p_\theta = l = mr^2\dot{\theta}$ is constant, and the period is $T_0 = 2\pi mr_0^2/l$. For $\beta > 0$ and $r \simeq r_0$

$$mr_0^2\dot{\theta} \simeq l\left[1 + 4\beta\left(p_r^2 + \frac{l^2}{r_0^2}\right)\right] \geqslant l(1 + 4\beta p_0^2), \tag{15}$$

with $p_0^2 = \frac{l^2}{r_0^2}$. In a time interval Δt, $\Delta\theta \gtrsim \frac{2\pi\Delta t}{T_0}(1 + 4\beta p_0^2)$, and, when $\Delta t = T_0$, we have the lower bound

$$\Delta = \Delta\theta - 2\pi \simeq 8\pi\beta p_0^2. \tag{16}$$

The orbital period T is also altered by GUP. For a $\Delta\theta = 2\pi$, the relative variation

$$\delta T = T/T_0 - 1 \simeq -4\beta p_0^2 \tag{17}$$

is compared with the numerical calculation in figure 2(b).

To outline the link with general relativity, we compare our result with the analysis of the precession of the perihelion of Mercury, as originally considered by Einstein [31–33]. We consider a nearly circular orbit and write the orbit equation starting from the conservation of energy in equation (9). By using $\mathrm{d}r/\mathrm{d}\theta = p_r r^2/l$ from equation (10), and $u = 1/r$ we have

$$H = \frac{l^2}{2m}(\mu + 2\beta l^2\mu^2) + \tilde{V}(u), \tag{18}$$

with $\mu \equiv (\mathrm{d}u/\mathrm{d}\theta)^2 + u^2$ and $\tilde{V}(u) = V(1/u)$. By deriving equation (18) one obtains, at the lowest order in β

$$\frac{\mathrm{d}^2u}{\mathrm{d}\theta^2} + u = -\frac{m}{l^2}\tilde{V}'(u)(1 - 4\beta l^2\mu) \tag{19}$$

with $\tilde{V}'(u) = \mathrm{d}\tilde{V}/\mathrm{d}u$. Equation (19) for $\beta = 0$ furnishes the orbit equation [67]; for $\beta > 0$, an additional contribution to the effective potential perturbs the orbit. Equation (19) is written as

$$\frac{\mathrm{d}^2u}{\mathrm{d}\theta^2} + u = -\frac{m}{l^2}\tilde{V}'(u) + \beta\mathcal{F}\left(\frac{\mathrm{d}u}{\mathrm{d}\theta}, u\right) \tag{20}$$

with

$$\mathcal{F} = 4m\mu\tilde{V}'(u) = 4m\left[\left(\frac{\mathrm{d}u}{\mathrm{d}\theta}\right)^2 + u^2\right]\tilde{V}'(u) \tag{21}$$

representing the perturbation due to the modified uncertainty principle, which disappears for $\beta = 0$.

For a nearly circular orbit $u \simeq (1/r_0)$, and a parabolic potential $\tilde{V}(u) = m\Omega^2/(2u^2)$, the first term in the right hand side of (20) $-m\tilde{V}'(u)/l^2 = m^2\Omega^2/(l^2u^3)$ is nearly a constant, and plays the role of the gravitational field. This shows the way the kinetic term induces an effective force, as general relativity induces a correction to the Newton force.

In a perturbative expansion in β, $\mathcal{F}$ in (20) produces a driving force term, as detailed in the following; such a term is in perfect analogy with the Einstein analysis of the Mercury orbit. We consider the solution for $\beta = 0$ representing an elliptical orbit with eccentricity e:

$$u_0 = \sqrt{\frac{m\Omega}{l}}[1 + e\cos(2\theta)]. \tag{22}$$

Equation (22) is valid for the parabolic potential, similar results are obtained for other potentials as, for example, the Newtonian gravitational potential. The perihelion corresponds to maximal u for $\theta_n = n\pi$ with $n = 0, 1, 2, \ldots$.

For $\beta > 0$, one adopts a perturbative expansion at the lowest order in the eccentricity e and β. The perturbation force $\mathcal{F}$ reads

$$\mathcal{F} = \mathcal{F}\left(\frac{\mathrm{d}u_0}{\mathrm{d}\theta}, u_0\right) \simeq -4m^{3/2}\Omega^{3/2}l^{1/2}[1 - e\cos(2\theta)]. \tag{23}$$

The perturbed orbit equation (20) is

$$\frac{\mathrm{d}^2u}{\mathrm{d}\theta^2} + u = \frac{m^2\Omega^2}{l^2u^3} + 4\beta\Omega^{3/2}m^{3/2}l^{1/2}[1 - e\cos(2\theta)]. \tag{24}$$

The forcing term in (24) is directly corresponding to the term obtained by Einstein representing the correction to the orbit due to general relativity. One can solve equation (24) at the lowest order in β and e as

$$u = \sqrt{\frac{m\Omega}{l}}\{1 - \beta m\Omega l + e[\cos(2\theta) + \beta\Omega ml\theta\sin(2\theta)]\}. \tag{25}$$

By writing equation (25) as

$$u \simeq \sqrt{\frac{m\Omega}{l}}\left\{1 - \beta m\Omega l + e\cos\left[2\theta\left(1 - \frac{\beta m\Omega l}{2}\right)\right]\right\}, \tag{26}$$

one sees that the maximum of u in equation (26) occurs for

$$\theta_n = n\pi\left(1 + \frac{\beta m\Omega l}{2}\right). \tag{27}$$

Hence the perihelion shifts for each half-orbit by an amount $\pi\beta m\Omega l/2$. Being $l \cong m\Omega r_0^2$ for nearly circular orbits, this result is consistent with the estimate above within numerical factors due to the definition of the precession angle. Equation (27) shows that the effect accumulates as the precession angle grows with n.

5. Geodesic formulation

It is instructive to write the previous results in a geodesic formulation [69]. We give in the following the expression of Φ and τ in our case.

We introduce in equation (10) the proper time τ by

$$\frac{\mathrm{d}t}{\mathrm{d}\tau} = \frac{1}{1 + 4\beta\left(p_r^2 + \frac{l^2}{r^2}\right)}. \tag{28}$$

In terms of τ, equation (10) read

$$\begin{aligned} &\frac{\mathrm{d}\theta}{\mathrm{d}\tau} = \frac{l}{mr^2}, \frac{\mathrm{d}p_\theta}{\mathrm{d}\tau} = 0, \\ &\frac{\mathrm{d}r}{\mathrm{d}\tau} = \frac{p_r}{m}, \frac{\mathrm{d}p_r}{\mathrm{d}\tau} = -\frac{\partial}{\partial r}\left[\Phi(r) + \frac{l^2}{2mr^2}\right], \end{aligned} \tag{29}$$

where Φ is a modified potential given by the solution of the equation

$$\frac{\partial\Phi}{\partial r} = \frac{1}{1 + 4\beta\left(p_r^2 + \frac{l^2}{r^2}\right)}\frac{\partial V}{\partial r}. \tag{30}$$

The expression for Φ is found at the lowest order in β by using the energy conservation $H = E$. After equation (9) we have

$$\beta\left(p_r^2 + \frac{p_\theta^2}{r^2}\right) \simeq 2m\beta E - 2\, m\beta V + o(\beta), \tag{31}$$

which, used in (30), gives at the lowest order in β

$$\Phi = V(1 - 8m\beta E) + 4m\beta V^2 \simeq V + 4m\beta V^2, \tag{32}$$

where we have used the term $m\beta E \ll 1$, as we are studying the perturbation to Newtonian dynamics (with generic potential) and the energy is also a small quantity. In the analogy with general relativity, this corresponds to consider a particle with energy much smaller than the rest energy mc^2, with c the vacuum light velocity.

For the proper time in (33), we have

$$\frac{\mathrm{d}t}{\mathrm{d}\tau} \simeq 1 + 8m\beta V, \tag{33}$$

which shows how the time speeds up at large r for a parabolic potential, hence the local velocity decreases, and this causes the precession of the orbit.

The geodesic formulation of the (29) is found by defining $x^0 = t, x^1 = r$ and $x^2 = \theta$, so we have

$$\frac{\mathrm{d}^2x^\alpha}{\mathrm{d}\tau^2} + \Gamma^\alpha_{\beta\gamma}\frac{\mathrm{d}x^\beta}{\mathrm{d}\tau}\frac{\mathrm{d}x^\gamma}{\mathrm{d}\tau} = 0, \tag{34}$$

where Greek indices span $0, 1, 2 = t, r, \theta$. The non-vanishing Christoffel symbols are

$$\Gamma^1{}_{00} = \Gamma^r{}_{tt} = \frac{1}{m}\frac{\partial\Phi}{\partial r}, \Gamma^1{}_{22} = \Gamma^r{}_{\theta\theta} = -r, \Gamma^2{}_{12} = \Gamma^2{}_{21} = \Gamma^\theta{}_{r\theta} = \frac{1}{r}, \tag{35}$$

and the (equation (34)) read explicitly as

$$\frac{\mathrm{d}^2x^0}{\mathrm{d}\tau^2} = 0 \frac{\mathrm{d}^2x^1}{\mathrm{d}\tau^2} + \Gamma^1_{00}\left(\frac{\mathrm{d}x^0}{\mathrm{d}\tau}\right)^2 + \Gamma^1_{22}\left(\frac{\mathrm{d}x^2}{\mathrm{d}\tau}\right)^2 = 0$$
$$\frac{\mathrm{d}^2x^2}{\mathrm{d}\tau^2} + 2\,\Gamma^2_{12}\frac{\mathrm{d}x^1}{\mathrm{d}\tau}\frac{\mathrm{d}x^2}{\mathrm{d}\tau} = 0. \tag{36}$$

Equation (29) with τ and Φ are the Newtonian limit of the relativistic particle with metric [69].

$$\mathrm{d}s^2 = -(1 + 2\Phi)\,\mathrm{d}\tau^2 + \frac{1}{1 + 2\Phi}\,\mathrm{d}r^2 + r^2\,\mathrm{d}\theta^2. \tag{37}$$

A similar approach, but in a quantum framework, is developed in [70], and allows to find the link between equation (37) and the SE in (6). Other solutions to the same problem are given in [71, 72] for cosmological descriptions of a homogeneous, isotropic universe. We describe the free particle, whose motion is described by geodesic equation, through a field $\psi(t,\ \mathbf{r})$ such that $|\psi(t,\ \mathbf{r})|^2$ is the probability to find the particle in the position $\mathbf{r}$ at time t. It must be governed by

$$\nabla^2_g\psi = -k_\mu k^\mu\psi, \tag{38}$$

where $\nabla^2_g = \frac{1}{\sqrt{g}}\frac{\partial}{\partial x^\mu}\left(\sqrt{g}\,g^{\mu\nu}\frac{\partial}{\partial x^\nu}\right)$ is the Laplacian operator in a curved spacetime. Specifically, equation (38) rules the motion of a particle with kinetic energy $K = \frac{\hbar^2}{2m_0}k_jk^j, j = 1, 2, 3$, mass at rest m_0, and relativistic momenta $p_\mu = \hbar k_\mu = \left(-\frac{E}{c},\ \mathbf{p}\right)$, $p^\mu = \hbar k^\mu = \left(\frac{E}{c},\ \mathbf{p}\right)$. It turns out that $k_\mu k^\nu = -\frac{E^2}{\hbar^2c^2} + \frac{2m_0K}{\hbar^2} = -\left(\frac{m_0c}{\hbar}\right)^2$. The next step is to find a metric tensor $g_{\mu\nu}$ such that, through a covariant transformation, equation (38) is equivalent to equation (6) in a flat space, that is, the particle moves under the effect of a gravitational parabolic potential. This has been already done for a spherical potential [70], and in the Newtonian limit $K \ll m_0c^2$, the metric in (37) is recovered. Extensions to the parabolic potential are possible and already explored via another scheme of derivation [71, 72], and will be treated in a general context in future works.

From $g_{\mu\nu}$, two important results are soon attained: the link between Einstein field equations and the SE [72], and the GUP effects in the quantization of the curved space [73]. Einstein equations are $G_{\mu\nu} = \frac{8\pi G}{c^4}T_{\mu\nu}$, with stress-energy tensor $t_{\mu\nu} = (\rho + p)\,U_\mu U_\nu - pg_{\mu\nu}$ of a perfect fluid of density ρ at pressure p. U_μ is the four velocity. The quantization of the curved space follows from the canonical commutation relations $[x^\mu,\ p^\nu] = \imath\hbar g^{\mu\nu}$ [73]. These, when transformed in the previous variables, must give equation (5), and thus the dependence of the metric tensor on β.

6. Numerical solution of the non-paraxial SE

We validate our theoretical analysis on the generalized SE equation (2) in two dimensions. We adopt dimensionless coordinates $s = t/t_N, u = x/w_N, v = y/w_N$, with $w_N^2 = \hbar t_N/m$, and $t_N = \Omega^{-1}$ and we have from equation (2)

$$\imath\partial_s\varphi = \frac{1}{2}\nabla^2_{uv}\varphi + \frac{\varepsilon}{8}\nabla^4_{uv}\varphi + \frac{1}{2}(u^2 + v^2)\varphi, \tag{39}$$

with $\nabla^2_{u,v} = \partial^2_u + \partial^2_v$, and $\varepsilon = 8m\Omega\beta\hbar$. $\varepsilon = 0$ corresponds to the conventional paraxial regime. At $t = s = 0$, a Gaussian wave-packet with waist w_o is the initial condition:

$$\varphi(u,\ v,\ s = 0) = \varphi_o\mathrm{e}^{-\left(\frac{u-u_o}{\sqrt{2}w_o}\right)^2 - \left(\frac{v}{\sqrt{2}w_o}\right)^2}\mathrm{e}^{\imath k_l v}. \tag{40}$$

In (40), the angular momentum is $l = \hbar k_l u_0$. If $\varepsilon = 0$ and $k_l = 0$, the wave-packet oscillates without orbiting in the y-direction (not reported). Figure 3(a) shows the evolution, for $\varepsilon = 0$ and $k_l = 20$, by various snapshots of $|\varphi|^2$: the bottom panel reveals the elliptical orbit. When $\varepsilon = 0.01$, as in figure 3(b), we have evidence of the predicted precession. Figure 3 shows representative simulations, similar results occur for all the considered cases. Figure 4(a) shows a volumetric visualization of the solution of equation (39) for a longer timescale with respect to figure 3, for $\beta = \varepsilon = 0$. Panels in figure 4 give the trajectories of the wave-packet center of mass, which, for $\varepsilon = 0$ do not reveal any precession. Figure 4(b) for $\varepsilon > 0$ demonstrates the precession and the reduction of the orbital period.

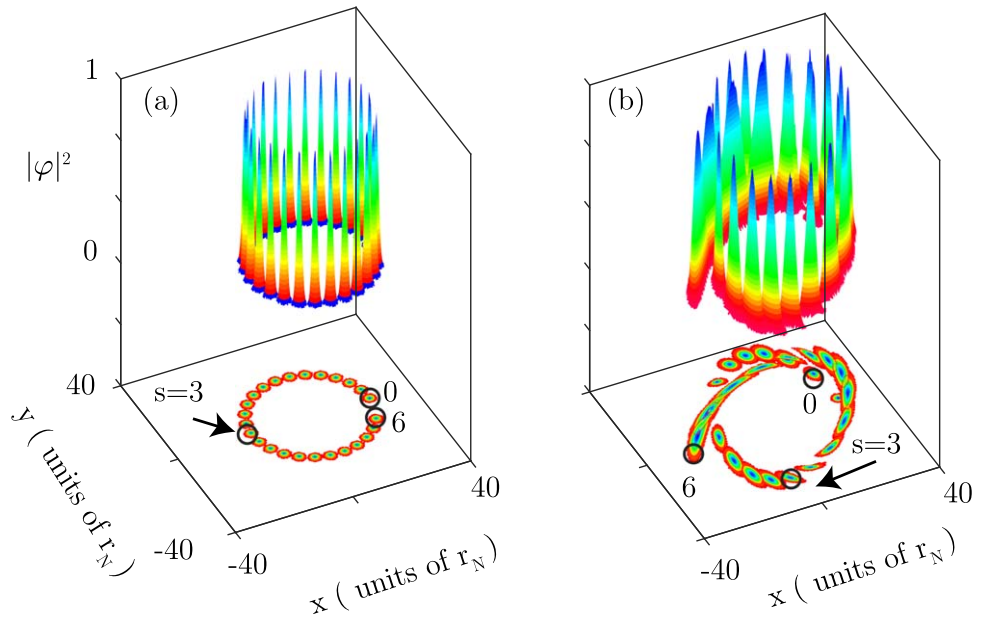

Figure 3. (a) Snapshots of $|\varphi|^2$ at different instants $s = t/t_N$ in the first orbit when $\varepsilon = 0$; (b) as in (a), for $\beta > 0$ ($\varepsilon = 0.01$). The panels show a two-dimensional visualization of $|\varphi|^2$ normalized to the maximal value. A precession occurs in the presence of the non-paraxial perturbation (parameters $u_o = 20, w_o = 0.1, k_l = 20$, longer evolution is shown in figure 4).

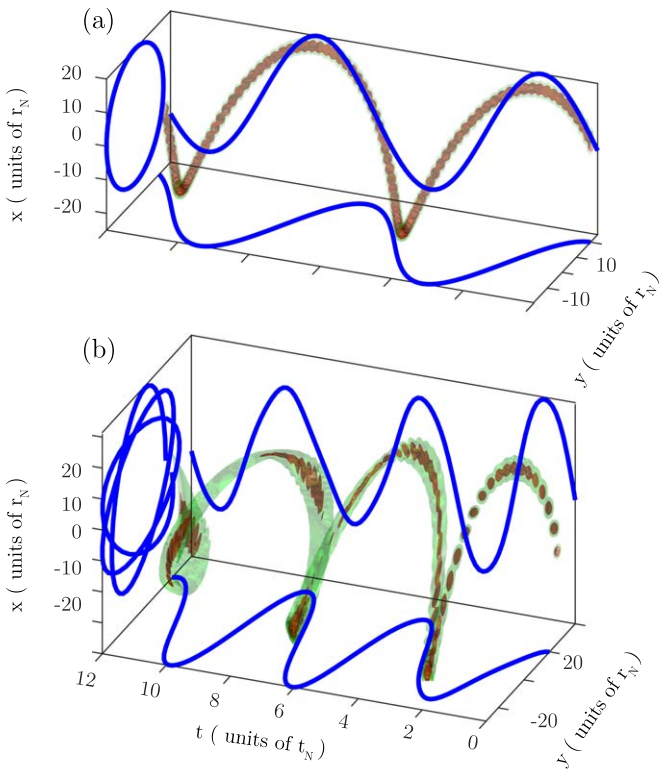

Figure 4. (a) Isosurface of the quantum fluid wave-packet orbiting in the parabolic potential in the absence of GUP effects ($\varepsilon = 0.00$); (b) as in (a) in the presence of GUP effects ($\varepsilon = 0.01$). The panels show orthographic projections of the center-of-mass trajectories determined by the wave-function (parameters $u_o = 20, w_o = 0.1, k_l = 20$).

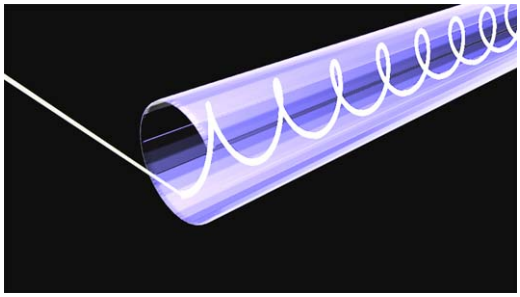

Figure 5. Graphical representation of a possible experiment by a graded index fiber, or highly non local nonlinear medium, which is excited by a tilted laser beam, which generates a spiraling state rotating with a period depending on the input angle.

7. Precession in analogs and real experiments with quantum fluids

To analyze possible experimental tests, we recall that β is typically expressed in terms of the dimensionless

$$\beta_0 = \beta \frac{\hbar^2}{\ell_p^2} = \beta M_{\rm P}^2 c^2, \tag{41}$$

with $M_{\rm P}$ the Planck mass, and c the vacuum light velocity. According to some authors, $\beta_0 < 10^{34}$ that we adopt as an optimistic upper bound for a real test of GUP phenomenology [45, 74]. For emulations, e.g. by paraxial light, we have $\beta_0 = 10^{55}$ [52, 54].

We consider a wave-packet at initial distance r_0 from the center of the potential with tangential velocity v_0 and $|l| = mv_0 r_0 = p_0 r_0$. For a harmonic trap, the quantum fluid size is $\ell_B^2 \cong \hbar/m\Omega$ [65], and we take $r_0 \cong \ell_B$. A key point here is that the precession angle and the delay with respect to the unperturbed case ($\beta = 0$) increase at any orbit. Hence, the longer the observation time, the more accessible the measurement of the predicted perturbation. For a 1-degree precession, the number of orbits is $\mathcal{N}_1 = \pi/(180\Delta) = \left(\frac{M_{\rm P}c}{mv_0}\right)^2/(1440\beta_0)$. With $\beta_0 = 10^{34}$, $\ell_B = 100\ \mu$m, and $v_0 = 10^{-10}c$, for ^{87}Rb BEC, we have $\mathcal{N}_1 \simeq 10^{18}$ orbits occurring in a time interval $\mathcal{N}_1 T_0 \simeq 10^{15}$ s, which is experimentally inaccessible. On the contrary, if we consider a photonic condensate simulation, with $\beta_0 = 10^{55}$, $m = 10^{-36}$ kg, and $v_0 = c$ [27], we have $\mathcal{N}_1 = 0.03$: an experimentally testable 30-degrees precession in $T_0 = 2$ ps.

Very interesting is the measurement of the time delay. For example, one can measure the delay of the orbital oscillation with respect to a metrological reference clock. The period shrinks at any orbit by a relative amount $\delta T = -4\beta_0\left(\frac{mv_0}{M_P c}\right)^2$. For ^{87}Rb BEC, we have $\delta T \simeq -10^{-20}$: after 10^6 orbits (15 h of observation), one has a delay of 1fs. The bounds for the modifications of the uncertainty principle become more precise when increasing the observation time. In the photonic simulation, one has 0.1 ps delay for 1 orbit.

We remark that in order to observe the precession, one has to generate states with an initial angular momentum in a trapping potential, as in equation (40). Considering the fact that our model applies to many physical systems, as in photonics, polaritonics, and BECs of atoms and photons, we remark that different approaches to realize experiments may be taken into account.

The literature and the experimental realizations of beams and condensates with angular momentum is so vast that cannot be reviewed here (see for example [75]). We will discuss in the following some representative cases.

For optical propagation, a trapping transverse parabolic potential is realized by graded index systems, as lenses or optical fibers. A further possibility is to consider an array of optical lenses, which, as shown in [76], may also emulate a parabolic medium. A further possible framework is given by highly nonlocal nonlinear optical systems, as thermal media, where related studies have been reported [77, 78].

In these devices, the initial state with angular momentum in equation (40) is excited by a beam spatially displaced with respect to the center of the trapping potential with an initial phase tilt (a sketch is given in figure 5). The angular momentum is varied by the incidence angle with respect to the input plane. The beam follows a motion described by an optical orbit as represented in our theoretical analysis and in the simulations in figure 4. As a representative case, one can consider a beam with a transverse size of the order of few microns, with 1 μm wavelength. The propagation length in fibers can be kilometers, this may enable a precise monitoring of the spiraling trajectories, and the deviation from an elliptical orbit due to the precession is here predicted.

For atomic BEC, states with angular momentum have been reported in a large number of articles (the interested readers may consider the references in [75]). The preparation of the initial state is conceptually similar to the optical case discussed above. In a wide trapping potential, a fraction of condensed atoms is launched with

an angular momentum parallel to the trap axis. This results into a spiraling motion of the atoms. An interesting possibility for putting atom into rotation is using transfer of orbital angular momentum from photons by stimulated Raman processes with Laguerre–Gauss optical beams, as, e.g. analyzed in [79]. This approach creates persistent currents in superfluid Bose gases, and the observation of precession dynamics in these systems may provide evidence of the effects discussed in this manuscript.

The case of *polaritonic condensates* is particularly relevant, as the generation of states with angular momentum has been actively investigated in recent years. For example, authors in [80] demonstrated that angular momentum can be transferred to an exciton-polariton BEC by an external incoherent pump. In a parabolic potential, which is always present in this class of condensates, one can generate a rotating motion, and correspondingly observe the predicted precession. Recent developments [81] show that it is possible to precisely control the amount of optical angular momentum, and the generation of various spinning states. These results show that the observation of the precession here predicted is within current technologies for polariton superfluids.

As further possible experimental framework, we mention the case of photonic BECs. [82] We are not aware of the experimental generation of photonic BEC with angular momentum. One can however figure out approaches similar to those discussed above for polaritonic BEC. Angular momentum may be transferred by an external pump to the condensate. A further possibility is adopting symmetry breaking microcavities (e.g. by axicon mirrors) to generate spinning photonic BECs. The detailed analysis of these possibilities is beyond the scope of this manuscript.

8. Conclusions

The longtime observation of an orbiting quantum fluid is a feasible experimental road to realize analogs of orbital precession effects in general relativity and post-Newtonian corrections to the gravity law. We predict that the orbit of a wave-packet in a trapping potential exhibits a precession with an intriguing connection with the well-known anomalous precession of the perihelion of Mercury, the first experimental test of general relativity. We show that the precession is also linked to the modification of the uncertainty principle predicted by the most studied theories of quantum gravity. The resulting non-commutative geometry, for which the momentum and the position in different directions do not commute, is derived from general relativity and interpreted in the quantum framework of a massive particle under a parabolic potential. The link between its motion equations and the corresponding geodesic equations for a free particle in a bonding gravitational field connects the quantum theory to the general relativity. Moreover, the analogy with the original Einstein's solutions addresses the existence of additional effective quantum forces occurring at the Planck scale.

With reference to feasible real laboratory tests of quantum gravity theories, the perturbation to the orbital period duration may become accessible after a large number of orbits because of the cumulative amplification during time. In photonic analogs, one can have $\beta_0 \simeq 10^{55}$, and quantum simulations and experiments with non-paraxial light, or polaritonic condensates, are well within current experimental possibilities. By quantum simulations, one may test the mathematical models, and also conceive improved frameworks for real probes of Planckian physics. This is specifically relevant for theories based on non-commutative coordinates [34], for which experiments are lacking.

Acknowledgments

This publication was made possible through the support of a grant from the John Templeton Foundation (grant number 58277). We also acknowledge support the H2020 QuantERA ERA-NET cofund Quomplex (grant number 731473) and H2020 PhoQus project (grant number 820392), Sapienza Ateneo (2016 and 2017), PRIN 2017 PELM (Grant number 20177PSCKT).

ORCID iDs

Giulia Marcucci https://orcid.org/0000-0001-7166-3643
Claudio Conti https://orcid.org/0000-0003-2583-3415

References

[1] Hossenfelder S 2013 *Living Rev. Relativ.* **16** 2
[2] Amelino-Camelia G 2001 *Phys. Lett.* B **510** 255
[3] Gambini R and Pullin J 1999 *Phys.Rev.* D **59** 124021

[4] Mukhanov V F and Winitzki S 2007 *Quantum Effects in Gravity* (Cambridge: Cambridge University Press)
[5] Rovelli C and Vidotto F 2015 *Covariant Loop Quantum Gravity* (Cambridge: Cambridge University Press)
[6] Thiemann T 2007 *Modern Canonical Quantum General Relativity* (Cambridge: Cambridge University Press)
[7] Kiefer C 2012 *Quantum Gravity* (Oxford: Oxford University Press)
[8] Maselli A, Pani P, Cardoso V, Abdelsalhin T, Gualtieri L and Ferrari V 2018 *Phys. Rev. Lett.* **120** 081101
[9] Garay L J, Anglin J R, Cirac J I and Zoller P 2000 *Phys. Rev. Lett.* **85** 4643
[10] Marino F, Ciszak M and Ortolan A 2009 *Phys. Rev.* A **80** 065802
[11] Vocke D, Maitland C, Prain A, Wilson K E, Biancalana F, Wright E M, Marino F and Faccio D 2018 Optica **5** 1099–103
[12] Steinhauer J 2016 *Nat. Phys.* **12** 959
[13] Faccio D 2012 *Contemp. Phys.* **53** 97–112
[14] Unruh W G 1976 *Phys. Rev.* D **14** 870–92
[15] Ornigotti M, Bar-Ad S, Szameit A and Fleurov V 2018 *Phys. Rev.* A **97** 013823
[16] Chä S-Y and Fischer U R 2017 *Phys. Rev. Lett.* **118** 130404
[17] Eckel S, Kumar A, Jacobson T, Spielman I B and Campbell G K 2018 *Phys. Rev.* X **8** 021021
[18] Paredes A and Michinel H 2016 *Phys. Dark Universe* **12** 50
[19] Zeng H, Wu J, Xu H and Wu K 2006 *Phys. Rev. Lett.* **96** 083902
[20] Barcelo C, Liberati S and Visser M 2003 *Phys. Rev.* A **68** 053613
[21] Longhi S 2011 *Appl. Phys.* B **104** 453–68
[22] Braidotti M C and Conti C 2017 arXiv:1708.02623
[23] Gentilini S, Braidotti M C, Marcucci G, DelRe E and Conti C 2015 *Sci. Rep.* **5** 15816
[24] Marcucci G and Conti C 2016 *Phys. Rev.* A **94** 052136
[25] Bohm A 1999 *Phys. Rev.* A **60** 861
[26] Carusotto I and Ciuti C 2013 *Rev. Mod. Phys.* **85** 299–366
[27] Klaers J, Vewinger F and Weitz M 2010a *Nat. Phys.* **6** 512
[28] Calvanese Strinati M and Conti C 2014 *Phys. Rev.* A **90** 043853
[29] Dominici L *et al* 2015 *Nat. Commun.* **6** 8993
[30] Amo A, Lefrère J, Pigeon S, Adrados C, Ciuti C, Carusotto I, Houdré R, Giacobino E and Bramati A 2009 *Nat. Phys.* **5** 805
[31] Einstein A 1915 *Erklarung der Perihelwegung Merkur der allgemeinen Relativitatstheorie* (Berlin: Koniglich Preussische Akademie der Wissenschaften)
[32] Kox J and Schutman R (ed) 1996 *The Collected Papers of Albert Einstein* (Princeton, NJ: Princeton University Press)
[33] Wisner C W, Thorne K S and Wheeler J A 1973 *Gravitation* (San Francisco, CA: Freeman)
[34] Connes A 1994 *Noncommutative Geometry* (New York: Academic)
[35] Kempf A, Mangano G and Mann R B 1995 *Phys. Rev.* D **52** 1108–18
[36] Garay L J 1995 *Int. J. Mod. Phys.* A **10** 145
[37] Kempf A and Mangano G 1997 *Phys. Rev.* D **55** 7909
[38] Witten E 1996 *Phys. Today* **49** 24
[39] Maggiore M 1993 *Phys. Lett.* B **319** 83
[40] Amelino-Camelia G 2013 *Phys. Rev. Lett.* **111** 101301
[41] Douglas M R and Nekrasov N A 2001 *Rev. Mod. Phys.* **73** 977
[42] Ghosh S 2014 *Class. Quantum Grav.* **31** 025025
[43] Scardigli F 1999 *Phys. Lett.* B **452** 39
[44] Chang L N, Minic D, Okamura N and Takeuchi T 2002 *Phys. Rev.* D **65** 125028
[45] Das S and Vagenas E C 2008 *Phys. Rev. Lett.* **101** 221301
[46] Pedram P 2012 *Phys. Lett.* B **714** 317–23
[47] Pikovski I, Vanner M R, Aspelmeyer M, Kim M S and Brukner C 2012 *Nat. Phys.* **8** 393–7
[48] Bekenstein J D 2012 *Phys. Rev.* D **86** 124040
[49] Bawaj M *et al* 2015 *Nat. Commun.* **6** 7503
[50] Silagadze Z 2009 *Phys. Lett.* A **373** 2643
[51] Pedram P, Nozari K and Taheri S H 2011 *J. High Energy Phys.* JHEP03(2011)093
[52] Conti C 2014 *Phys. Rev.* A **89** 061801
[53] Castellanos E and Escamilla-Rivera C 2017 *Mod. Phys. Lett.* A **32** 1750007
[54] Braidotti M C, Musslimani Z H and Conti C 2017 *Physica* D **338** 34
[55] Braidotti M C, Conti C, Faizal M, Dey S, Alasfar L, Alsaleh S and Ashour A 2018 *Europhys. Lett.* **124** 44001
[56] Chin C, Grimm R, Julienne P and Tiesinga E 2010 *Rev. Mod. Phys.* **82** 1225
[57] Longhi S 2018 *Opt. Lett.* **43** 226
[58] Das S and Vagenas E C 2009 *Can. J. Phys.* **87** 233–40
[59] Briscese F, Grether M and de Llano M 2012 *Europhys. Lett.* **98** 60001
[60] Mercati F, Mazón D, Amelino-Camelia G, Carmona J M, Cortés J L, Induráin J, Lämmerzahl C and Tino G M 2010 *Class. Quantum Grav.* **27** 215003
[61] Benczik S, Chang L N, Minic D, Okamura N, Rayyan S and Takeuchi T 2002 *Phys. Rev.* D **66** 026003
[62] Brau F 1999 *J. Phys. A: Math. Gen.* **32** 7691
[63] Brown L S 1972 *Am. J. Phys.* **40** 371
[64] Vleck J H Van 1928 *Proc. Natl Acad. Sci.* **14** 178
[65] Dalfovo F, Giorgini S, Pitaevskii L and Stringari S 1999 *Rev. Mod. Phys.* **71** 463–512
[66] Landau L D and Lifshitz E M 2013 *Quantum Mechanics: A Shorter Course of Theoretical Physics* (Amsterdam: Elsevier)
[67] Goldstein H 1965 *Classical Mechanics* (Harlow: Pearson)
[68] Rauschenbakh V, Ovchinnikov M Y M Y and McKenna-Lawlor S M P 2002 *Essential Spaceflight Dynamics and Magnetospherics* (Berlin: Springer)
[69] Misner C W, Thorne K S and Wheeler J A 2017 *Gravitation* (Princeton, NJ: Princeton University Press)
[70] Suda M 2016 *J. Mod. Phys.* **7** 523
[71] Rosen N 1993 *Int. J. Theor. Phys.* **32** 1435
[72] Capozziello S, Feoli A and Lambiase G 2000a *Int. J. Mod. Phys.* D **9** 143
[73] Capozziello S, Lambiase G and Scarpetta G 2000 *Int. J. Theor. Phys.* **39** 15

[74] Lambiase G and Scardigli F 2018 *Phys. Rev.* D **97** 075003
[75] Yao A M and Padgett M J 2011 *Adv. Opt. Photonics* **3** 161
[76] Yariv A 1991 *Quantum Electronics* (San Diego, CA: Saunders College)
[77] Marcucci G, Pierangeli D, Gentilini S, Ghofraniha N, Chen Z and Conti C 2019 *Adv. Phys.* X **4** 1662733
[78] Marino F 2019 arXiv:1908.00875
[79] Helmerson K, Andersen M, Ryu C, Cladé P, Natarajan V, Vaziri A and Phillips W 2007 *Nucl. Phys.* A **790** 705c
[80] Dall R, Fraser M D, Desyatnikov A S, Li G, Brodbeck S, Kamp M, Schneider C, Höfling S and Ostrovskaya E A 2014 *Phys. Rev. Lett.* **113** 200404
[81] Boulier T, Cancellieri E, Sangouard N D, Glorieux Q, Kavokin A V, Whittaker D M, Giacobino E and Bramati A 2016 *Phys. Rev. Lett.* **116** 116402
[82] Klaers J, Schmitt J, Vewinger F and Weitz M 2010b *Nature* **468** 545